On Porosity Formation in Metal Matrix Composites Made with Dual-Scale Fiber Reinforcements Using Pressure Infiltration Process

REIHANEH ETEMADI, KRISHNA M. PILLAI, PRADEEP K. ROHATGI, and SAJAD AHMAD HAMIDI

This is the first such study on porosity formation phenomena observed in dual-scale fiber preforms during the synthesis of metal matrix composites (MMCs) using the gas pressure infiltration process. In this paper, different mechanisms of porosity formation during pressure infiltration of Al-Si alloys into Nextel™ 3D-woven ceramic fabric reinforcements (a dual-porosity or dual-scale porous medium) are studied. The effect of processing conditions on porosity content of the ceramic fabric infiltrated by the alloys through the gas PIP (PIP stands for ''Pressure Infiltration Process'' in which liquid metal is injected under pressure into a mold packed with reinforcing fibers.) is investigated. Relative density (RD), defined as the ratio of the actual MMC density and the density obtained at ideal 100 pct saturation of the preform, was used to quantify the overall porosity. Increasing the infiltration temperature led to an increase in RD due to reduced viscosity of liquid metal and enhanced wettability leading to improved feedability of the liquid metal. Similarly, increasing the infiltration pressure led to enhanced penetration of fiber tows and resulted in higher RD and reduced porosity. For the first time, the modified Capillary number (Ca^*), which is found to predict formation of porosity in polymer matrix composites quite well, is employed to study porosity in MMCs made using PIP. It is observed that in the high Ca^* regime which is common in PIP, the overall porosity shows a strong downward trend with increasing Ca^*. In addition, the effect of matrix shrinkage on porosity content of the samples is studied through using a zero-shrinkage Al-Si alloy as the matrix; usage of this alloy as the matrix led to a reduction in porosity content.

DOI: 10.1007/s11661-015-2792-9

I. INTRODUCTION

IN pressure infiltration process (PIP) for making metal matrix composites (MMCs), liquid metal is injected under pressure into a mold packed with reinforcing fibers. PIP is very similar to the resin transfer molding (RTM) process, which is used for the manufacture of near-net-shaped parts out of polymer matrix composites.[1] Both are characterized as liquid molding processes and consist of the following steps: (1) Dry fiber preforms made out of fabrics or fiber mats are placed in the mold. (2) Liquid matrix (monomeric thermosetting resin such as unsaturated polyesters or epoxies for PMCs, and molten metal or alloys for MMCs) is injected into the preform. (3) The liquid is allowed to harden through temperature control of the mold (exothermic thermosetting reaction for the resin and phase change for the metal). (4) The final net-shaped composite part is removed from the mold. An important advantage of the liquid infiltration processes is the production of near-net shape composite parts from preforms designed using different reinforcements for optimal mechanical and other properties.[2,3] The use of the woven or stitched fabrics as reinforcements is increasing as they provide a convenient way of improving the mechanical properties by ensuring higher fiber volume fractions through clustering of fibers as fiber tows or bundles. Porosity* is a major defect found in these fabricated composites which adversely affects their fatigue properties.

Of the two types of PIPs, we will be studying the gas PIP (gas pressure infiltration process) where a pressurized gas is used to push the liquid metal into the dry preform. The processing conditions have a major influence on the porosity content of MMC composites synthesized by the gas PIP. Another major source for porosity formation during this process is solidification shrinkage, which happens during the metal phase

*In this study, the term ''void volume fraction'' is used to quantify the void space inside a preform as a fraction of the total preform volume, while the presence of voids inside the composite will be referred to as the ''porosity.''

REIHANEH ETEMADI, Graduate Student, and KRISHNA M. PILLAI, Associate Professor, are with the Department of Mechanical Engineering, University of Wisconsin-Milwaukee, Milwaukee, WI 53211. Contact e-mail: retemadi@uwm.edu PRADEEP K. ROHATGI, Professor, is with the Department of Material Science and Engineering, University of Wisconsin-Milwaukee. SAJAD AHMAD HAMIDI, Research Associate, is with the Department of Civil and Environmental Engineering, University of Wisconsin-Milwaukee.

Manuscript submitted May 18, 2014.
Article published online February 18, 2015

change. In the present study, the effect of changes in the processing parameters of infiltration temperature and pressure on the porosity content of MMC samples synthesized by gas PIP is studied. In addition, the effect of matrix shrinkage on the porosity content of MMC samples is explored using a zero-shrinkage alloy as the matrix. The phenomenon of porosity formation during the making of MMC using PIP from 3D-woven reinforcements (classified as dual-scale porous media in the next section) has not been addressed in the literature. However, one can find large literature on porosity formation mechanisms in such dual-scale reinforcements during the manufacture of polymer matrix composites using RTM, which, as mentioned before, is very similar to PIP used for the synthesis of MMCs.

To study the mechanisms of porosity formation in MMCs reinforced with 3D-woven fabrics, a thorough understanding of the physics of infiltration process is necessary. After a review of research done so far in the simulation and modeling of PIP, and the similar RTM process (which is the pre-requisite to understanding porosity formation mechanisms), a brief review of the research conducted on porosity formation in MMCs will be presented. The review reveals a gap in the literature, in terms of the theoretical/computational explorations and experimental investigations, on the effects of the dual-scale nature of woven, braided or stitched fabrics used as reinforcement in MMCs on metal flow in PIP and the resultant porosity formation. Thus, in this study, results of a series of experiments, conducted using the gas PIP for making MMC samples after varying the material and process parameters, will be presented. The effects of the processing parameters, such as the infiltration pressure (*i.e.*, the net pressure applied on the infiltrating metal), the infiltration temperature (*i.e.*, the temperature of the infiltrating metal), and the matrix shrinkage, on porosity formation in MMC samples are studied.

A. *Modeling Flow Through Dual-Scale Fiber Mats and Porosity Formation During RTM Processing of Polymer Matrix Composites*

Woven and stitched fabrics inherently induce a dual-scale flow behavior since they comprise of distinct macro- and micro-flow regions, each with different impregnation/flow rates corresponding to the different permeability values. The pores of the macro-region (to be also called the inter-tow region as it comprises the large spaces found between fiber tows and bundles) are much bigger and will fill more rapidly, while the pores in the microscopic region (to be also called the intra-tow region as it comprises the smaller pores found between individual fibers inside the tows) will saturate more slowly. This order-of-magnitude difference in the pore-length scales in the same medium is the basis for their classification as a "dual-scale" porous medium.[4] Due to the delay that occurs in the complete saturation of the preform, the distinction between these separate macro- and micro-flow regions is important. The macro-flow front first fills the more permeable pores between the tows, and then the fluid from this region fills the less permeable pores within the tows. At this point, the more slowly advancing micro-flow front dictates the filling progress. Therefore, in a dual-scale porous medium, the location of the macro-flow front seldom coincides with the boundary of the fully saturated region of the preform. For these preforms, a partially saturated region exists behind the macro-flow front in which the pores of the inter-tow region may be filled but the fiber tows are still just partially filled. In case of the one-dimensional overall flow created in a preform, a partially saturated length, L_s, can be defined as the distance between the macro-flow front and the fully saturated secondary 'front' as shown in Figure 1.[1,5] This partially saturated length decreases as the intra-tow permeability of fiber tows gets closer to the inter-tow permeability. The coexistence of these micro- and macro-flows due to the dual-scale nature of the preform has well-documented effects on resin flow during the RTM processing such as the porosity formation[1,6,7] and the existence of a partially saturated region behind the flow front.[1,8–12]

Many RTM mold-filling simulations have been developed in an effort to optimize the mold-filling process and to avoid incomplete filling of RTM molds and the resultant dry spots or porosity formation in composites. These numerical simulations are accomplished by incorporating the fundamental balance laws for the conservation of mass, momentum, energy, and species into the physics of resin flow through the fibrous preform. In most LCM simulations, the flow of resin is considered as the flow of a Newtonian fluid through *a single-scale* porous medium. It is also assumed that a sharp front exists between the wet and dry portions of the porous medium during infiltration, and the flow behind the front is considered fully saturated. With this assumption, the following equations {Darcy's law, Eq. [1]; Continuity Equation, Eq. [2]} for single-phase flow are applicable for modeling the resin flow:

$$V = -\frac{K}{\mu} \cdot \nabla p \qquad [1]$$

$$\nabla \cdot V = 0. \qquad [2]$$

Here, V is the volume-averaged Darcy velocity, K is the permeability tensor for the preform, μ is the viscosity, and p is the pore-averaged resin pressure.[4] Note that the gravity term in Darcy's law is ignored as this term is small in the high-pressure infiltration conditions found in PIP and RTM molds. Using the quasi steady-state approximation, the pressure distribution behind the front can be calculated using an elliptic equation, which is obtained by substituting the expression for Darcy velocity from Eq. [1] in the continuity equation, Eq. [2]:

$$\nabla \cdot \left(\frac{K}{\mu} \cdot \nabla p \right) = 0. \qquad [3]$$

The resin flow is a non-isothermal flow due to the single or multiple exothermic chemical reactions occurring as the resin state changes from liquid to solid during its curing. Since the resin viscosity has a dependence on both the resin temperature and the state of resin cure, the equations for predicting resin temperatures and resin cure in the

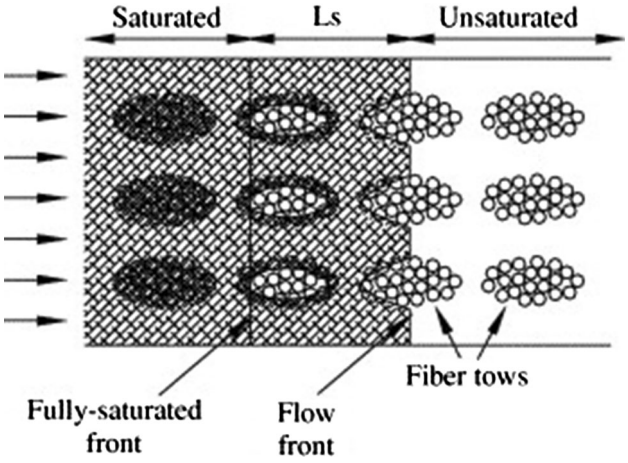

Fig. 1—A schematic diagram depicting the saturated, partially saturated (L_s), and unsaturated flow regions within dual-scale preforms, and highlights the delayed impregnation of the fiber tows Ref. [1].

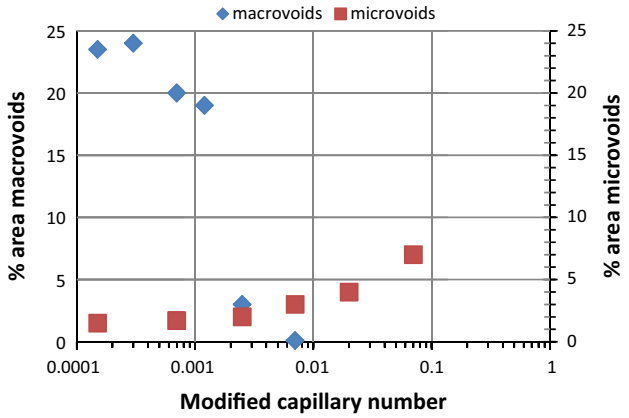

Fig. 2—Percent area macro- and micro-voids as a function of modified capillary number in RTM (This approximate graph is based on the information provided in Ref. [23].).

preforms have also to be solved simultaneously. (These equations are not listed here, but have been described in detail by Dessenberger and Tucker[13].) However, this physics developed for single-scale porous media characterized by a mono-modal pore-size distribution is not applicable to the case of woven or stitched fabrics, which are characterized as dual-scale porous media and are marked by a bi-modal pore-size distribution. For example, during resin flow in RTM, the dual-scale media exhibit the presence of unsaturated regions behind the resin front, thus violating the main assumption of the preform being fully saturated, as required for the use of Eqs. [1], [2], and [3].

There have been several attempts to develop accurate, next-generation RTM mold-filling simulations for the dual-scale preforms.[1,4,14,15] When the resin is flowing through such a media, it faces less resistance in the large pores between fiber tows than in the micro-pores inside fiber tows, so it goes quickly around the tows and fills up the large pores before starting to penetrate the tows. These tows continue to absorb liquid after the macroscopic resin front has passed, acting like sinks of liquid in the macroscopic flow field. To describe such flows, a new mass balance equation has been proposed with a nonzero sink function on the right-hand side of Eq. [2][4,16]:

$$\nabla \cdot v = -S. \qquad [4]$$

Here S is the sink function equal to the volumetric rate of liquid absorption.[1,4,14,15]

Voids** in polymer matrix composites are formed when air bubbles are cast into the final composite in the form of permanent air pockets. Since the presence of bubbles signifies incomplete saturation of pore space by resin, the process of bubble formation and movement can be explained in terms of the unsaturated flow. Many experimental investigations have been conducted to study the mechanism of bubble formation at the microscopic level.[17–21] Bubble formation during the RTM process is mainly caused by mechanical trapping of air (due to incomplete removal of air from between the fiber space during resin flow) rather than the presence of volatiles in the resin. Patel *et al.*[17] and Chen *et al.*[22] identified two basic types of bubbles or voids: (1) macro-voids, which are formed between the fiber bundles, and (2) micro-voids which are formed inside the tows. The formation of voids was correlated with the capillary number, Ca {given later in Eq. [6], Section III–B}: for $Ca < 0.01$, the formation of macro-bubbles is predominant as the wicking flow inside the tows is faster than the inter-tow flow; for $Ca > 0.01$, the creation of micro-bubbles is dominant since the inter-tow flow overtakes the wicking flow inside the tows.[17] As shown in Figure 2, $Ca = 0.01$ corresponds to a minimum in the percentage of voids formed during infiltration and forms the most optimum condition for resin injection in the mold.

Many authors have developed "tow impregnation" models to predict the micro-void formation inside fiber bundles. In many of these models, fiber tows are modeled as porous cylinders, which are impregnated radially by a micro-front of resin after the macr-ofront has quickly engulfed the surrounding gap region. Parnas and Phelan[1] used this concept to develop the flow equation for dual-scale fabrics where they predicted cylindrical air bubbles, following the ideal gas law, forming inside the tows as a result of the micro-front movement. Fang and Advani used the same approach and predicted a rather unrealistic, almost uniform distribution of voids in a 1-D LCM mold,[24] while the actual bubble distribution is like a step function near the macroscopic front.[7] Chan and Morgan also predicted void formation in a bi-directional mat.[14] Chen, Macosko, and Davis used the simplistic linear impregnation physics of Washburn to propose a similar model[22] which could qualitatively predict the off-centered, non-cylindrical voids seen in the experiments.[20] Chang and Hourng used Darcy's law in both the intra- and

**The term "void" used in the polymer matrix composite community is equivalent to the term "porosity" used in the metal matrix composite community, and represents the dry spots present in the matrix after the processing of the composite.

inter-tow regions to numerically study the bubble formation in cylindrical tows.[25] These models have some deficiencies such as (1) the absence of any physics for bubble mobilization and (2) the assumption of cylindrical geometry for the tows (rather unrealistic since tows in woven fabrics are like wavy thick threads with elliptical cross sections); such deficiencies lead to unrealistic void-distribution predictions.

The formation and migration of bubbles near the flow front is an indication of a two-phase (resin and air) flow through the porous media and can be explored within the classical theoretical framework for multiphase flows in porous media. Hahn *et al.* used a transient mass balance equation for the diffusion of saturation to predict the distribution of saturation near a very slow-moving front.[26] Mohan *et al.* developed a pure finite element-based algorithm for mold filling in LCM using the concept of fill factor which is similar to saturation while they assumed a zero pressure for the unsaturated region.[27] As mentioned before, Patel *et al.* conducted a series of studies on bubble creation and migration[17] and linked the dual-scale nature of fiber mats to the types of bubbles observed near the flow front. They observed formation of *small micro-bubbles* (or micro-voids) inside the tows at high resin velocities when the macro-front in the gaps was ahead of the capillary pressure-driven micro-front inside the tows. They also observed the formation of *large macro-bubbles* (or macro-voids) in the inter-tow gaps at low resin speeds when the micro-front inside the tows was ahead of the macro-front in the gaps. Patel and Lee modeled the bubble formation using a two-channel model while using the conventional equations for multiphase flow.[28,29] Their model was quite successful in the prediction of macrobubble distribution at very slow speeds, but not in the prediction of micro-bubbles at relatively rapid resin injections typical of the RTM process. Departing from the usual tow-based models, Pillai and Advani qualitatively predicted the formation and migration of bubbles at the macroscopic level using the ''shock'' in the transient saturation distribution predicted by the Buckley-Leverette (B-L) equation.[30] The B-L formulation is a first-order hyperbolic equation and is based on the two-phase flow of resin and air in single-scale porous media, which included the generalized Darcy's law for averaged momentum balance and a transient saturation-based equation for mass balance. Chui *et al.* later applied the same B-L formulation numerically and were able to predict the step-like porosity distribution observed near the macroscopic flow fronts in fabrics.[31]

B. *Porosity Formation During Pressure Infiltration Process in Metal Matrix Composites*

As mentioned before, the liquid metal infiltration process in PIP for the fabrication of MMCs is very similar to the RTM process used for the manufacture of polymer matrix composites. It consists of the injection and subsequent solidification of liquid metal within interstitial spaces of a fibrous preform, which is a very complex process. Currently, the liquid-state processes are preferred to other manufacturing techniques for MMC production as they are more economical while benefiting from the advantages of well-proven casting processes. It should be mentioned here that *MMCs produced by pressure infiltrations are considered to be in the category of* cast *composites.*

According to metallurgists and material scientists, essentially three classes of phenomena govern the infiltration process: fluid flow and 'capillarity,' transport/mechanical phenomena, and heat flow and solidification.[32] The capillary forces (governing the 'capillarity') dictate the initial path of the flowing liquid metal inside the preform. Transport phenomena during infiltration govern the temperature and solute distributions at and behind the infiltration front. Often mechanical compression of the preform also happens during infiltration and finally, the solidification of the metal matrix creates the final MMC part. All these phenomena, including metal and heat flow, species transport, preform deformation, segregation of alloying elements, chemical reactions at the metal-fiber interface, and so on, happen during the infiltration of metal into the dry preform. As a result, for realistic simulation of the process, the PIP must be modeled in a coupled, multi-dimensional manner. During the past few decades, many researchers have tried to develop mathematical models and numerical simulations to predict and understand the flow during the PIP process to improve the quality of infiltration. The first and perhaps the most comprehensive attempt to model PIP can be attributed to Mortensen *et al.*[33] The traditional equations for single-phase flow in porous media (Darcy's law and the continuity equation) were employed to develop an analytical model for fluid flow and heat transfer during infiltration of fibrous preforms by a pure metal. The model was based on several simplifications including the ''slug flow'' or sharp-front flow assumption, which means that the pore space behind a clearly defined front is saturated with metal, while the previously existing air has been squeezed out ahead of the front. After applying these simplifications, some analytical solutions were developed for the temperature and porosity distributions during a simple 1-D infiltration.

Numerical models have been developed to predict the appearance of defects in the end products and optimize the mold design and processing parameters. PIP mold-filling simulations have been confined to single-scale porous media so far, and the verified flow effects in dual-scale fiber mats such as absorption/trapping of liquid metal by fiber tows or other possible flow effects such as premature freezing of metal after coming into contact with colder tows have not yet been studied. However, the use of woven or stitched fabrics (dual-scale porous media) is increasing as they provide a convenient way of improving the mechanical properties of MMCs through the inherently higher fiber volume fractions. As mentioned in the previous section, research in RTM has shown that there are some clear discrepancies between the numerical predictions based on the single-scale

porous media models and the experiment observations of flow in dual-scale fabrics. Although significant research has been done to model resin flow and void formation in dual-scale preforms, *no equivalent work has been done in PIP to study the effect of dual-scale nature of the preform on metal flow and subsequent porosity formation*. Only recently, Wang and Pillai[34] developed a numerical simulation for pressure infiltration of dual-scale preforms. They addressed the dual-scale nature of the preform by assigning different permeabilities and void volume fractions to the inside (intra-tow) and outside (inter-tow) regions while using the same governing equations. Their results show an irregular flow front in dual-scale fabrics and an unsaturated region behind the front due to the formation of gas pockets inside the fiber tows.

Due to the complexity of defect formation mechanisms in the synthesis of MMCs by pressure infiltration, the production of porosity-free MMCs has remained a technical challenge. It has been demonstrated that the porosity defects are deleterious to the mechanical properties of cast MMCs and are adversely affected by the porosity content of the composite casting.[35–37] The control of such casting defects should be achieved through optimization of the casting temperature, temperature of the mold, pressure, and cooling rate.[38] Another source of porosity formation is poor infiltration. Assuming a complete infiltration, the other important source of porosity is metal shrinkage during solidification.[37] This problem is tackled by employing directional solidification toward a riser in a temperature gradient or by applying very high pressure during solidification.[37] The porosity defect is more significant in composites with high volume fraction of reinforcement because the high volume fraction of reinforcement hinders the flow of interdendritic liquid as well as obstructs any bulk movement of the metal matrix in the semi-solid state during solidification. To avoid this defect, Al-Si alloys are recommended because of its good fluidity†[39] and its compatibility with several reinforcements.[37]

†Fluidity in metallurgical terms is a material's ability to flow into and fill a given cavity, as measured by the dimensions of that cavity under specified experimental conditions.

Apart from the normal casting porosity resulting from dissolved gases and shrinkage, there are additional causes related to the process. In cast composites, porosity can be classified into two types: (1) those away from the reinforcement inside the matrix and (2) those at the boundary of matrix and reinforcement. The second type of porosity is more undesirable because it leads to the debonding of the reinforcement from the matrix under low stress. In composites, gas porosity may nucleate heterogeneously on the surface of the reinforcement during solidification.[40] To summarize, the main sources of porosity formation in MMC castings are (1) Gas entrapment due to incomplete evacuation of the preform during infiltration, (2) 'Preporosity' formation due to incomplete infiltration, (3) Precipitation of inclusions and dissolved gas present in the melt, and (4) Solidification shrinkage.

Gas porosity can be present in a casting when there is dissolved gas in the molten metal or alloy together with the presence of favorable nucleation sites. Hydrogen is the only gas known to dissolve to any significant extent in molten aluminum. During solidification, the gas is rejected at the solid/liquid interface and enriched at the later stages of freezing. Gas precipitation will only occur in the presence of favorable nucleation sites as non-wetted or poorly bonded interfaces.[41,42]

Solidification shrinkage occurs when the pressure gradient is insufficient to overcome the resistance offered by the reinforcement and dendritic networks to feed voids formed by matrix shrinkage during phase change. In their study, Ghomy and Campbell[42] concluded that as the number of effective pore nuclei increases in a casting, the central internal macro-pores, caused by solidification shrinkage, will disperse into fine micro-pores and the porosity will convert from external to internal. Other factors such as surface roughness, interface wetting, reaction, and so on can also affect porosity[43] along with metal feedability.[44]

While considerable literature is available on porosity formation in unreinforced metals or alloys and in powder technology, relatively little has been done to investigate porosity formation in reinforced castings produced by infiltration processing. Notable examples of studies done on porosity formation in MMCs include the works of Ray,[40] Long *et al*.,[45] Samuel *et al*.,[44] and Emamy *et al*.[42] High pressures used in MMC production generally suppress porosity formation, but such defects were detected in MMCs made at moderate pressures (10 MPa/1450 psi) by Mortensen *et al*.[46] and high pressures (100 MPa/14.5 ksi) by Asthana.[47]

A study by Ilegbusi and Yang[48] investigated the effect of processing conditions and reinforcement characteristics, such as matrix alloying, reinforcement coating, and cooling condition, on the formation of local negative pressures and subsequent nucleation of shrinkage porosity after assuming a planar matrix/reinforcement interface in the pressure infiltration casting of metal matrix composites. Their results showed that the degree of susceptibility to porosity nucleation in the composite depends on the type of matrix/reinforcement system. For example, porosity nucleation in Al/Al_2O_3 system is found to be more energetically favorable than the Al/SiC system. The appropriate application of metal alloying, such as Mg in the Al/Al_2O_3 system and Mg and Cu in the Al/SiC system, or reinforcement coating such as Cu coating on SiC, significantly reduces the contact angle and improves the wettability at the interface enhancing infiltration by increasing the pressure barrier to porosity formation.‡ Increasing the void volume fraction of the preform as well as the reinforcement (particles/fibers) size also increases fracture

‡The pressure barrier to porosity nucleation is the minimum local pressure required to avoid porosity nucleation.

pressure[§] and improves the infiltration. They concluded

[§]A liquid subjected to negative pressure is metastable; the negative pressure at which bubbles from vapors form spontaneously is the fracture pressure. These bubbles grow until the system pressure rises to the equilibrium vapor pressure.

this means that there is a lower potential for porosity nucleation in fiber-reinforced composites, which typically have larger reinforcement size than particulates and whiskers. In another study, Ilegbusi and Yang[43] investigated the mechanisms of porosity nucleation (or bubble nucleation in the liquid state) on five interfacial configurations as shown in Figure 3 for a variety of matrix/reinforcement systems. They found that interfaces with negative curvatures such as the cavities are potential sites for porosity formation. Other effective methods to avoid porosity include careful control of the cooling condition as well as the applied pressure.

Calin *et al.*[49] studied the effects of fiber volume fractions (*fvf*) on porosity and thermal conductivity in Al-MgO particulate-reinforced MMCs of 5, 10, and 15 pct *fvf* produced by melt stirring. They observed that an increase in *fvf* leads to an increase in the porosity.

As commented earlier, the interface between the matrix and reinforcement has a crucial effect on the properties of MMCs which is affected during their fabrication. The interface-related problems, which are system-specific, include the interfacial chemical reaction, degradation of the reinforcement, and the lack of wettability with the matrix. The nucleation of pores in MMCs is strongly dependent on the matrix-reinforcement interface characteristics. The modification of interface properties, such as the addition of alloy elements to a metal matrix, has been experimentally shown to suppress porosity formation.[50] Another effective way for interface modification is the coating of reinforcement to improve the interface wettability.[51] Rajan *et al.*[52] reviewed the surface treatment methods and coating work carried out on reinforcements such as carbon/graphite, silicon carbide (SiC), and alumina (Al_2O_3), and their effects on the interface, structure, and properties of aluminum-alloy MMCs. The metallic coatings improve the wettability of the reinforcement, but change the matrix alloy composition by alloying with the matrix. Ceramic coatings reduce the interfacial reaction by acting as a diffusion barrier between the reinforcement and the matrix. Multilayer coatings have multiple functions, such as promoting wetting, acting as diffusion barrier, and releasing thermal residual stresses.

This brief literature review reveals that although significant research has been done on the phenomenon of bubble formation and migration in dual-scale preforms during the RTM processing of polymer matrix composites resulting in porosity in the final product, no equivalent research has been done so far to study the effect of the dual-scale nature of the preform on the metal flow during PIP and the resultant porosity caused by the delayed impregnation of the fiber tows in this type of preforms. Flow visualization using transparent Plexiglas molds, which is a popular technique to study resin flow in RTM, is not possible in PIP because of the very high temperatures encountered in the PIP mold. *This work is the first attempt to study the mechanisms of porosity formation during gas pressure infiltration of metal into dual-scale ceramic preforms, and to study the factors affecting these mechanisms*. The parameters affecting the infiltration process can be classified into five groups: (a) fiber-preform properties (related to unit-cell structure, void volume fraction, pore-size distribution, fiber, and tow dimensions), (b) liquid/metal properties (surface tension and viscosity), (c) solidification related (related to shrinkage, *etc.*), (d) liquid/solid interface properties (the contact angle, surface reactivity, *etc.*), and (e) experimental conditions {applied pressure, infiltration time (which is defined as the time during which the constant infiltration pressure is applied), temperature, and atmosphere of infiltration}.[47,53] The aim of this work is to investigate the effect of some of these parameters on the porosity content in the Al-Si alloys/3D-woven Nextel™ fabric infiltrated using the gas PIP. Effectiveness of a new dimensionless parameter called the modified capillary number, which includes some of those above-listed parameters in a dimensionless grouping, is also explored.

II. INSTRUMENTATION AND EXPERIMENTAL PROCEDURE

A series of experiments were conducted using the gas pressure infiltration process (*i.e.*, the gas PIP) to make MMC samples corresponding to different material and processing parameters. The effects of the above-mentioned parameters, such as infiltration pressure, infiltration temperature, and matrix shrinkage, along with the capillary number on the phenomenon of porosity formation in MMC samples were studied.

Molten aluminum alloy was infiltrated into preforms made of a 3D woven fabric using a pressurized gas in our PIP setup. 3M™ Nextel™ 720 ceramic fibers produced by 3M were woven by 3TEX Inc. into 3WEAVE®Non-crimp 3D Orthogonal Fiber Architecture as shown in Figure 5. The weave was cut into 2.3 in × 2.3 in (5.8 cm × 5.8 cm) square pieces and then heat cleaned by a specific process

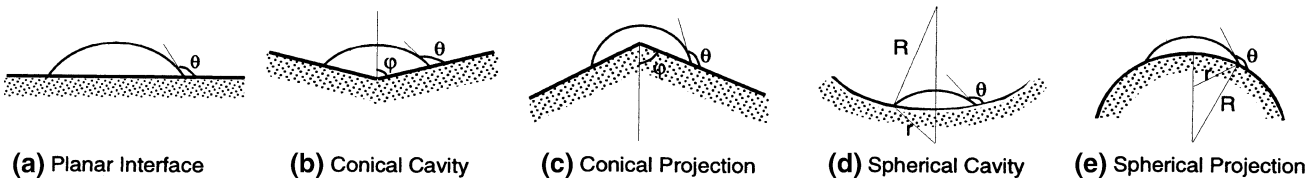

Fig. 3—Five different interfacial configurations studied for porosity nucleation in Ref. [43].

recommended by the manufacturer to remove the sizing and other contaminations. It was then placed at the bottom of a square steel tube which was used as the mold with cross-sectional dimensions of 2.3 in × 2.3 in (5.8 cm × 5.8 cm) and height of 5 in (12.7 cm). The inner surface of the mold was coated with a thin layer of graphite to avoid reactions between the metal and mold surface. Then a specific amount of the alloy was placed on top of the preform inside the mold. After that, the mold was placed inside our gas PIP apparatus (see Figure 4) which was then used for the gas pressure infiltration of Al alloys into the preforms. The pressure chamber is made of a 7 in (18 cm) inside diameter, 7.76 in (19.7 cm) outside diameter, and 10.83 in (27.5 cm) long steel cylinder. The lid assembly and the bottom portion of the chamber are made of 2014 Al alloy. The lid and steel cylinder have copper tubing for water cooling. The melting furnace composed of two semi-cylindrical heating elements. The apparatus can handle infiltration pressures up to 300 psi (2.07 MPa) through the pressurized inert Argon gas. After placing the mold inside the pressure chamber, the lid was closed and the vacuum pump was turned on to evacuate the furnace,[§§] and then the heater was set at the specified temperature. After reaching that temperature and waiting for an hour to equilibrate, the metal was infiltrated into the preform by applying gas pressure. In order to perform a constant-pressure infiltration experiment, the pressure was increased as fast as possible to the chosen value, and then it was kept constant for half an hour during the infiltration process. (This time is called the infiltration time which was kept constant during these experiments.) After this period, it was abruptly reduced to atmospheric pressure through the pressure-relief valve. Later, the lid was removed and the sample was left to cool down. The resulting MMC pieces were cut, and their densities were estimated as a measure of the porosity content in each sample. The fabricated samples were then further studied using the optical microscope and SEM. For this, the specimens cut from the castings were ground and polished using our automatic polishing equipment; the final polishing used the 0.25 μm silica colloid to obtain the best possible surface.

In this work, Al-Si alloys (A356 and Mercusil) were selected as the matrix materials for our MMCs made using the gas PIP. Their chemical compositions are shown in Table I. A356 alloy is an important alloy in automotive and other applications. Its density is 167.62 lb/ft^3 (2.685 g/cm^3), and its solidus and liquidus temperatures are 1031 °F and 1139 °F (555 °C and 615 °C), respectively. To study the effect of matrix shrinkage on the porosity content in the composite, a hypereutectic Al-Si alloy with zero volume shrinkage[54] was used as the matrix in some of our experiments. This alloy, called Mercusil, was made by stir casting, and its chemical composition was confirmed by ICP (inductive couple plasma) analysis. 3M™ Nextel™ 720 ceramic fibers, which were woven by 3TEX Inc into 3WEAVE®Non-crimp 3D Orthogonal Fiber Architecture as shown in Figure 5, was used as the preform for reinforcement purposes, and the main properties of its fibers are listed in Table II. The 3M™ Nextel™ 720 fiber, composed of 85 pct alumina and 15 pct silica, offers the lowest creep of any Nextel™ Fiber at temperatures up to 2102 °F (1150 °C).

As shown in Figure 5, the 3D weaving incorporates multiple layers of warp and fill yarns in a single fabric. In the non-crimp 3D orthogonal weaving, invented at North Carolina State University, the fabric composed of a number of warp and fill-direction tows, with the latter

[§§]Vacuum pressure could not be monitored due to the limitation of our setup. Moreover, it was difficult to maintain the vacuum due to leakage. Hence, very likely only partial vacuum was created inside the chamber.

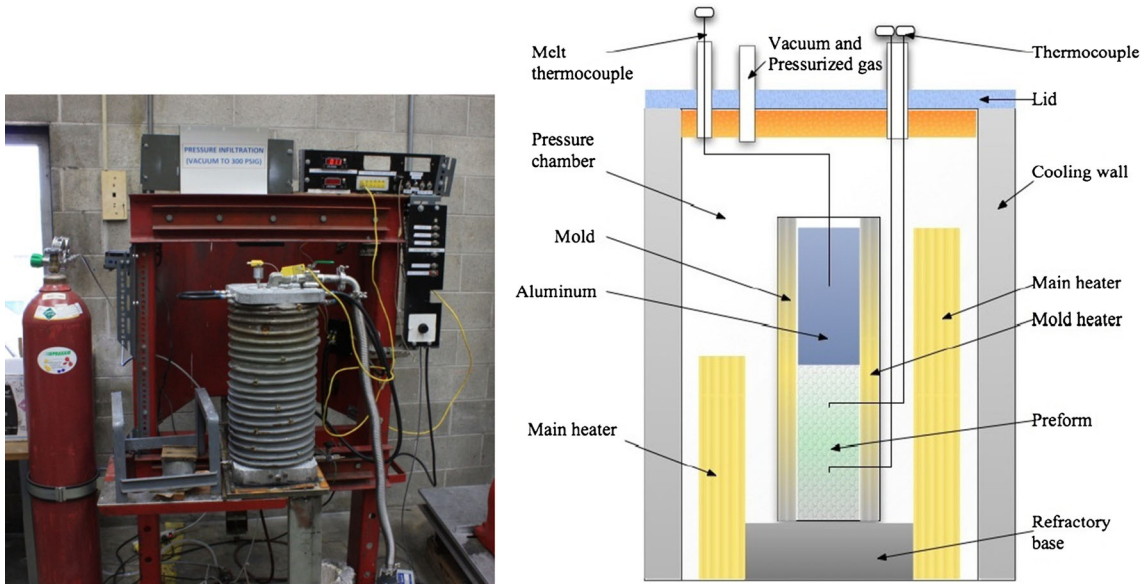

Fig. 4—Gas pressure infiltration equipment and its schematic.

Table I. Chemical Composition of Aluminum Alloys A356 and Mercusil

	Element (Wt. Pct)						
Alloy	Si	Mg	Ti	Fe	Cu	Mn	Al
A356	6.5-7.5	0.34	0.013	0.08			bal.
Mercusil	20-30	0.4-1.6		1.4	0.25	0.3	bal.

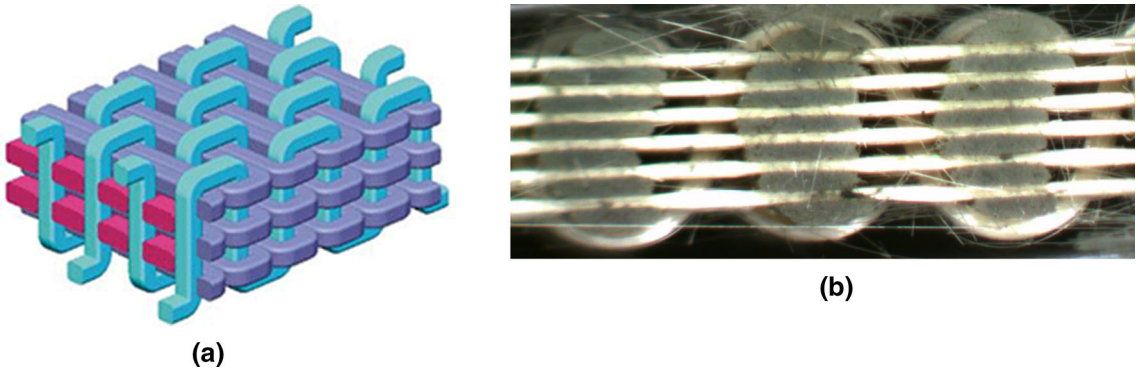

Fig. 5—(*a*) Non-crimp orthogonally woven alumina fabric with 3D weave pattern Ref. [55], (b) Longitudinal cross section of the 3D woven Nextel™ fabric.

Table II. Important Properties of 3M™ Nextel™ 720 Ceramic Fibers

Property	Unit	Nextel 720
Sizing color	color	green
Chemical composition	wt. pct	85 Al_2O_3 15 SiO_2
Melting point	celsius	1800
Filament diameter	μm	10-12
Crystal size	Nm	<500
Density	g/cc	3.40

being one more than the former. The yarns aligned in the length direction, called the Z yarns, traverse multiple fill and warp layers, looping over the top fill yarn, then going through the fabric thickness, and then going under the bottom fill yarn, and finally pulling the warp and fill layers together. The Z yarns thus create a 3-D weave pattern. The yarns consisting of 3M™ Nextel™ 720 fibers were used in this pattern to create the Nextel™ 3D fabric. The fabric thickness was approximately 3 mm, and its architecture was based on six warp yarns per inch, seven fill yarns per inch, and the Z yarns. A schematic of the weave pattern and a magnified cross section of the 3M's 3D-woven Nextel™ fabric are shown in Figure 5.

III. RESULTS AND DISCUSSION

The experiments conducted using the 3TEX Nextel™ preform infiltrated with A356 alloy at different pressures and temperatures are summarized in Table III. The initial void volume fraction of the Nextel™ weave was measured to be 65 pct. Each experiment Sij (Table III) was repeated three times. The density of the MMC samples, synthesized using gas PIP at different processing conditions specified in Table III, was measured with direct Archimedian method using the Mettler Toledo standard level analytical balance with its density determination kit. In this method, the density of MMC samples was determined with the aid of a reference liquid (here distilled water) whose density ρ_0 is known. The sample were weighed first in the air and then in the reference liquid. The density could be calculated from these two weights as

$$\rho = \frac{A}{A-B}(\rho_0 - \rho_L) + \rho_L, \qquad [5]$$

where ρ is the density of the MMC sample, A is the sample weight in the air, B is the sample weight in distilled water, ρ_0 is the density of the reference liquid, and ρ_L is the air density (0.0012 g/cm^3).

Then the relative densities were calculated, which were the actual densities as percentages of the theoretically maximum density (the latter defined as the ideal density of the MMC with the assumption that all the void volume in the preform is infiltrated with the metal). The results of the 3-sample averaging of densities as well as the scatter bars corresponding to 95 pct confidence level[¶] of the MMC samples are shown in Figure 7. As we can see, an increase in the temperature of the infiltrating metal as well as an increase in its pressure leads to the increase in the density of the samples. A detailed explanation of this phenomenon is given in the following section.

[¶]The 95 pct confidence level refers to the fact that the measured value of a sample is likely to fall within a certain band 95 times on the average out of 100.[56]

Table III. Some Details of the Experiments Conducted to Study the Effect of Infiltration Pressure and Temperature on the Quality of Infiltration and Porosity Content in the MMC Samples Created Using the Gas PIP

Sample No.	Infiltration Temperature (°C)	Infiltration Pressure (psi)	Density (g/cm^3)	Relative Density (Pct)
S11	750	100	1.60	54.63
S12	800	100	2.20	74.84
S13	850	100	2.45	83.59
S14	900	100	2.59	88.25
S21	750	200	1.83	62.24
S22	800	200	2.32	78.93
S23	850	200	2.54	86.54
S24	900	200	2.69	91.65
S31	750	300	2.27	77.23
S32	800	300	2.51	85.63
S33	850	300	2.65	90.18
S34	900	300	2.73	93.13

The sample numbers are in the form S_{ij} with i and j being the numerical values—note that i and j changes with the infiltration pressure and temperature, respectively.

A. *Effect of Processing Conditions on the Quality of Infiltration and Porosity Content*

Increases in the infiltration temperature and pressure are both effective means of achieving full infiltration. Let us discuss the effects of these two processing parameters in greater detail.

Many of the problems in the processing of metal matrix composites, such as poor wetting of the reinforcement by molten metal, are related to the interface between the metal and reinforcement.[57] The interfacial zone that links the reinforcement phase with the matrix phase can be either in the form of a single surface of atomic bonds (simple interface), or one (or even several) new reaction phases and simple interfaces located between the reinforcement and matrix. Most MMCs form non-equilibrium systems during processing—a chemical potential gradient exists at the matrix-reinforcement interface, and this gradient is the driving force for diffusion or chemical reactions at high temperatures during processing.[38] Desirable interfacial properties sometimes force contradictory demands. For example, high chemical affinity between the matrix and reinforcement is desired to ensure spontaneous combination of the two phases, yet low chemical affinity is desired to avoid unwanted chemical reactions at the interface during the processing. In general, wetting of the matrix-reinforcement interface can be classified into two broad categories based on the nature of attractive forces at the interface: (1) physical wetting and (2) chemical wetting. In polymer matrix composites, the physical wetting predominates, while in MMCs, both the physical and chemical wettings are important.

Increasing the infiltration temperature improves the quality of infiltration in two ways: Firstly, it improves the wetting between the matrix and the reinforcement, and thus decreases the contact angle. Secondly, it decreases the viscosity of the molten metal. These two affects facilitate the feeding of the liquid metal to regions undergoing solidification. This explains the gain in density, observed in Table III and Figure 7, of MMC samples with increasing infiltration temperatures.

Due to the dual-scale nature of the preform, the infiltrating liquid fills the pore spaces between the tows at a much faster rate than the filling of empty pore spaces within the tows[34] (See Figure 1). As a result, there will be two distinct types of flow fronts during infiltration: the first flow front corresponds to the gap (inter-tow) flow and is called the open (macro) flow front; the second type of flow fronts, which form gas pockets inside the tows, are called the closed (micro) flow fronts. These closed flow fronts are formed behind the open flow fronts and are surrounded by the melt. These macro- and micro-flows have a significant influence on infiltration and solidification during PIP. For example, they lead to the formation of a partially saturated region, rich in porosity, behind the open flow fronts. Because of the poor wettability of alumina by aluminum, a pressure greater than the thermodynamic gas pressure needs to be applied to the surrounding melt to infiltrate the fiber tows and eliminate the trapped porosity.[58]

The compression and disappearance of the gas pockets during infiltration is dependent on the local melt pressure around the gas pockets, which in turn is a function of the applied inlet pressure. Therefore, by increasing the inlet infiltration pressure, we are able to decrease the volume and number of gas pockets, which in turn led to lesser porosity content in the final product. As shown in Figure 6, the metal content inside the fiber tows increases as the infiltration pressure increases from 100 psi (0.69 Mpa) to 300 psi (2.07 Mpa). This increase in the tow saturations with infiltrations is reflected in the increasing sample densities as seen in Table III and Figure 7.

B. *Effect of Modified Capillary Number on Porosity Formation in MMC Samples*

Since the balance between viscous and capillary forces present during infiltration significantly affects the process, their relative importance can be assessed by means of the capillary number defined as the ratio of the two forces. Patel *et al.*, in their study of the RTM process for the synthesis of polymer matrix composites, demonstrated that porosity formation in dual-scale fibrous

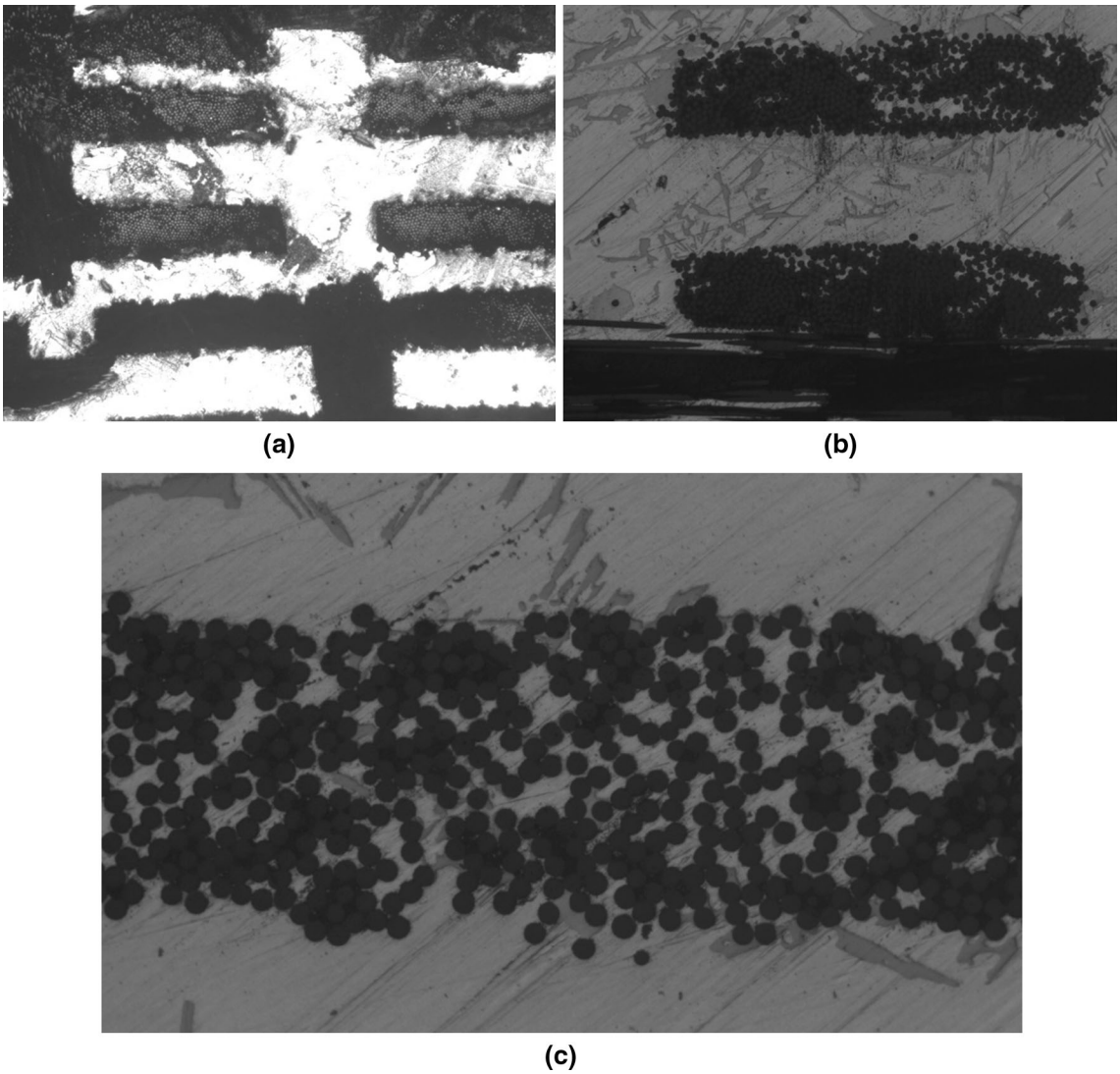

Fig. 6—Optical micrographs of the infiltrated fabric: (*a*) The 100 psi (0.69 Mpa) infiltration pressure case showing large gaps between fiber tows infiltrated with metal while almost no metal can be seen in the pores inside the fiber bundles due to low infiltration pressure. (*b*) By increasing the infiltration pressure to 200 psi (1.38 Mpa), some metal is observed to have infiltrated inside the fiber tows. (*c*) More metal infiltration occurred inside the tows as the pressure increases to 300 psi (2.07 Mpa). (Note that the bright areas in these figures correspond to the matrix while the dark areas represent either the fibers or empty voids between them.).

porous media can be correlated to a modified capillary number (Ca^*).[59] The porosity formation in such media involves two types of flows: flow through inter-tow gaps, and the capillary pressure-driven wicking of tows. Competition between these two flows created the lead-lag pattern or fingering in the main flow front. These flows were deemed to be dependent on the balance of viscous and capillary forces, and hence a modified Capillary number, Ca^*, representing the ratio of these forces in the flow field was proposed:

$$Ca^* = \frac{\mu \cdot V}{\sigma_{\mathrm{LM}} \cdot \cos\theta} \qquad [6]$$

Here μ is the viscosity of the liquid metal, V is the characteristic velocity of liquid metal in the mold, σ_{LV} is the surface tension of the liquid metal, and θ is the contact angle. Due to a lack of any means to directly measure metal velocity in the PIP mold cavity, the Darcy velocity at the middle of the mold-filling process was chosen as the characteristic melt velocity. This velocity was estimated using the 1-D form of Eq. [3] to determine an analytical expression for the pressure distribution, and then using it in Eq. [1] to estimate Darcy velocity at the center of the mold (see Appendix A for details). The permeability of the dual-scale preform, which is also required for these calculations, was estimated using the method described in Appendix B. Wang *et al.*[60] used an oscillating-cup viscometer to measure the absolute viscosities of molten metals at different temperatures and proposed the following empirical Arrhenius-type equation for the viscosity of A356 alloy at different temperatures:

$$\mu = \mathbf{A}\, e^{\mathbf{B}\cdot T^{-1}} \qquad [7]$$

Table IV. Some of the Properties of the Aluminum alloy A356 used in Our Calculations Ref. [41]

Material	σ (N/m)	Contact Angle θ	Volumetric Shrinkage (Pct)
A356	0.79	135	5.7

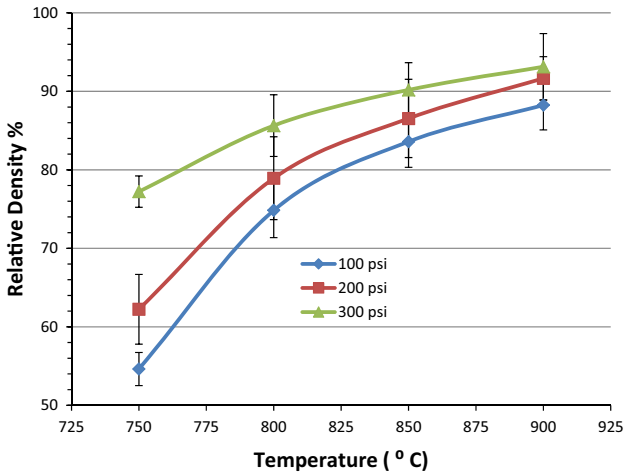

Fig. 7—Relative density of the MMC samples made using gas PIP increases with the infiltration temperature and pressure.

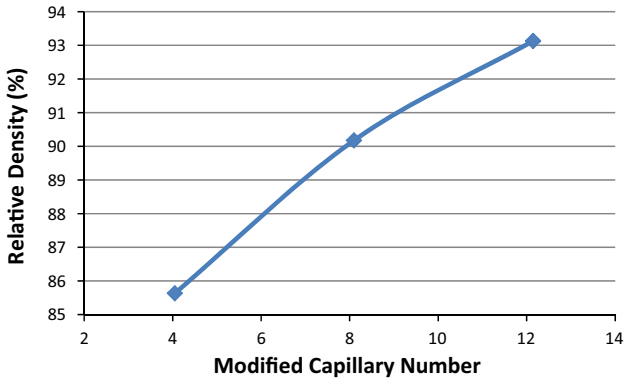

Fig. 8—Experimentally observed increase in the relative density with an increase in the modified capillary number, *Ca**.

Here T is the temperature of the alloy in Kelvin. For A356, **A** is 0.157 mPa·s, and **B** is 1850 K.[60] Equation [7] was used to estimate viscosities for A356 at different temperatures while calculating *Ca**. The other values needed for the modified capillary number calculations of Eq. [6] were extracted from References 41, 60, 61 (See Table IV).

Figure 8 shows the relative densities of the samples increasing with the modified capillary numbers. The high *Ca** in these experiments indicates that flow leads in the gaps between the axial tows and no macro-porosity is formed between tows. Micro-pores are formed inside the tows due to the axial wicking of the aligned tows from the inter-tow gaps (in-plane roundup type mechanism) and also due to the impregnation of transverse tows occurring after the liquid has flowed around the transverse tows (transverse roundup type mechanism).[59] Petal *et al.*, in this same study of void formation in LCM processes, found that the voids or air pockets formed inside the tows increased in number as *Ca** increased beyond 0.01[59] (See Figure 2). This observation is *contradicted* by the trend seen in Figure 8 where increase in the relative density is due to the increased saturation of tows. Such an unexpected result can be explained as follows. For the present set of experiments, the increase in *Ca** is directly related to the increase in the melt-front velocity through the preform (Eq. [6]), which in turn is directly proportional to the magnitude of the infiltration pressure (Eq. [15] of Appendix A). Therefore, the increase in *Ca** is directly caused by an increase in the infiltration pressure, and hence, the micro-bubbles trapped inside the tows shrink or even possibly disappear due to the dissolution of trapped air in the alloy melt. As a result, the trend seen in Figure 7 of increasing relative density with infiltration pressure is replicated in Figure 8 with relative density increasing with *Ca**.

C. *Effect of Matrix Shrinkage on Porosity in MMC Samples*

As mentioned in the introduction, the shrinkage that occurs on solidification is the primary source of porosity formation in solidifying castings. Solidification shrinkage is a contraction that occurs at the liquid-solid transition as a result of the more open atomic arrangement in liquid metals changing to the denser solid phase. In most cast alloys, the volume shrinkage is typically between 3.2 and 7.2 pct (See Eq. [19] of Reference 62). If a region of liquid in the casting becomes isolated from additional feed liquid, and then after solidification and shrinkage, the pressure in the liquid drops, causing an increasing pressure difference between the inside and outside of the casting. In this case, there are two possibilities: (i) internal shrinkage porosity may form in the presence of favorable nuclei and (ii) the solidified shell of the casting collapses plastically inwards leading to external porosity or sink.

To experimentally investigate the effect of matrix shrinkage on void fraction in MMC samples, a hypereutectic aluminum–silicon alloy called Mercusil, with chemical composition as shown in Table I, was used as the metal matrix. With this composition, the aluminum–silicon alloy system exhibits near-zero shrinkage on solidification.[54] Figure 9 shows the plot of the relative density of MMC samples resulting from a series of experiments where the samples infused with Mercusil alloy (at 200 psi (1.38 Mpa) infiltration pressure and under infiltration temperatures of (1023 K, 1073 K, 1123 K, and 1173 K) 750 °C, 800 °C, 850 °C, and 900 °C temperatures) are compared with the samples made from the A356 matrix under similar conditions.

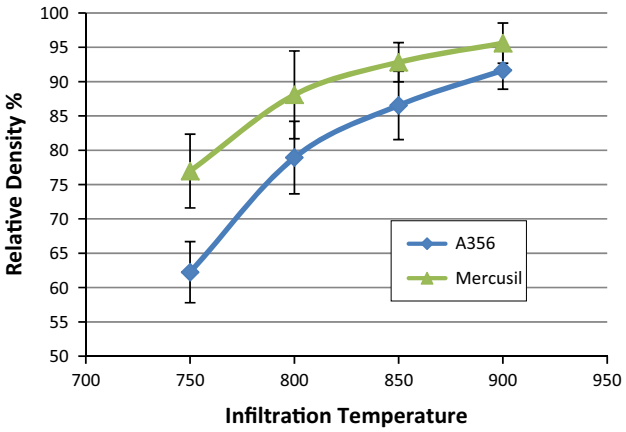

Fig. 9—A plot of Relative Densities as a function of infiltration temperature for pressure infiltration of 3D-Nextel™ fabric with A356 and Mercusil alloy at 200 psi (1.38 Mpa).

As the graph suggests, eliminating the shrinkage porosity results in density gain for MMC samples produced with Mercusil.

IV. SUMMARY AND CONCLUSIONS

An experimental study of porosity formation in MMCs, which were made using gas PIP with a dual-scale reinforcement, was conducted successfully. The effect of processing parameters of infiltration temperature and pressure on the porosity content of such MMC samples was investigated. The effect of dual-scale nature of the chosen 3D-woven ceramic fabric on metal flow during PIP was studied experimentally through micrographs prepared from samples created by infiltration of these preforms with Al alloy at different temperatures and pressures. A measure of average overall porosity was established through relative density, which can be defined as the ratio of the current MMC density to the hypothetical MMC density created by filling all the pore space with infiltrating metal. It was observed that at lower infiltration temperature and pressures, most of the fiber tows were not infused with metal and this caused high overall porosities in the samples. However, increasing these two parameters led to higher infiltrations and lower porosities in the samples. Increasing the infiltration pressure caused the gas pockets formed inside tows to shrink, while increasing the infiltration temperature caused lower viscosity of the metal and hence more metal wetting and improved feedability.

The porosity formation was also studied in terms of the parameter of modified Capillary number, *Ca**, used in the study of void formation in polymer composites made using RTM. For the estimation of *Ca**, the velocity of open or macro-front at the center of the preform was used. In the considered method of gas PIP with high *Ca** infiltration, the flow leads in gaps between the axial tows, and as predicted by previous observations, no macro-pores were formed. However, as observed in Reference 59, micro-pores were indeed formed inside the tows due to the delayed impregnation of metal into the aligned tows. Since the velocity of open or macro-front at the center of the preform was used in the estimation of *Ca**, the increase in the relative density with *Ca** is caused due to the increase in the infiltration pressure and subsequent shrinkage and disappearance of micro-pores inside the tow. This decrease in MMC porosity with an increasing *Ca** contradicted the trend of increasing void percentages with *Ca** seen in Reference 59. However, this study indicates that the parameter of modified Capillary number, Ca*, can be used to control porosity formation in MMCs produced using gas PIP.

In addition, it was shown experimentally that metal shrinkage plays an important role in porosity formation in this set of MMCs. At identical processing conditions, the use of a zero-shrinkage Al-Si alloy (Mercusil) resulted in higher densities in MMC samples compared with the samples produced using the regular A356 alloy.

ACKNOWLEDGMENTS

Helpful comments and assistance from Dr. Benjamin Schultz during the laboratory work for this study is greatly appreciated. Financial help from UWM graduate school, UW-Foundation and Army Research Lab (Aberdeen) is gratefully acknowledged.

APPENDICES

Appendix A: Calculating Darcy Velocity for modified Capillary Number

The superficial velocity used in Eq. [6], which is the average velocity of metal inside the preform, can be estimated by assuming the infiltration process to be a line injection in a flat rectangular mold. This is a 1-D boundary value problem with time-dependent moving boundary. For simplicity, we assume that there is full saturation behind the moving front and the preform is an isotropic medium. The governing differential equations for this problem are Eqs. [1] and [2], which are Darcy's law and the continuity equation, respectively. For the 1-D case, these equations reduce to

$$q = -\frac{K}{\mu}\frac{dp}{dx} \qquad [8]$$

$$\frac{dq}{dx} = 0 \qquad [9]$$

Combining these equations, the governing equation for pressure distribution is given by

$$\frac{d^2p}{dx^2} = 0. \qquad [10]$$

The general solution to this equation is

$$p(x) = Ax + B \qquad [11]$$

with A and B as arbitrary constants. The domain is from $x = 0$ at the entrance to $x = x_f(t)$ at the liquid front in the mold with x_f being the x coordinate of the liquid front. We solve this problem for $0 \le x \le x_f(t)$ with the following pressure boundary conditions:

$$p(x = 0) = p_{in} = \text{const.}$$

$$p(x = x_f) = 0.$$

Here, p_{in} is the infiltration pressure applied to the incoming melt. Note that we ignore any suction pressure at the liquid front in this estimate. Applying these boundary conditions to Eq. [11] results in $B = p_{in}$ and $A = \frac{-p_{in}}{x_f(t)}$.

On substituting A and B in Eq. [11], we will have the equation for melt pressure distribution in the wetted preform as

$$p(x,t) = -\frac{p_{in}}{x_f(t)}x + p_{in} = p_{in}\left(1 - \frac{x}{x_f(t)}\right). \quad [12]$$

In calculating the modified capillary number for each experiment (Eq. [6]), the typical velocity was taken as the front velocity, which was estimated when the front has reached the middle section of the preform. From Eq. [12], the pressure distribution, when the front reaches the at mid-section, is

$$p(x) = p_{in}\left(1 - \frac{x}{T/2}\right), \quad [13]$$

where T is the flow-direction length of the preform. Hence, the pressure gradient in the wetted portion of the PIP preform at the liquid front is given as

$$\left.\frac{dp}{dx}\right|_{x=T/2} = \frac{p_{in}}{T/2}. \quad [14]$$

Now the front velocity, v_f, is obtained by dividing the Darcy velocity at the front with the void volume fraction, ε, as

$$v_f = \frac{dx_f}{dt} = \frac{q(x_f)}{\varepsilon} = \frac{K}{\varepsilon\mu}\frac{p_{in}}{T/2} \quad [15]$$

Appendix B: Estimation of Permeability for Fiber Preform

To estimate Ca^* in Eq. [6], an estimate of Darcy velocity at the mold center is needed, and for which an estimation of the permeability, K, of the 3D weave Nextel™ fabric used in the present study is required. If we assume the preform to be single-scale porous medium, Kozeny-Carman equation can be used to calculate the preform permeability as

$$K = D_f^2\phi(\varepsilon), \quad [16]$$

where D_f is the fiber diameter, ε is the void volume fraction of the preform, and ϕ is defined by the equation

$$\phi(\varepsilon) = \frac{1}{180}\cdot\frac{\varepsilon^3}{(1-\varepsilon)^2}. \quad [17]$$

However, in determining the permeability of a dual-scale fabric, the size of pores between the tows, the diameter of the fibers inside the tows, and the architecture of the preform, all play a role. Since the 3D Nextel™ fabric is of dual-scale type, the analytical correlation presented by Papathanasiou[63] for dual-scale porous media was applied to calculate the permeability of the preform. In this model, the boundary element method (BEM) was used to simulate Stokes flow across hexagonal arrays of unidirectional fiber tows in which the individual filaments are packed in hexagonal or square arrangements inside the tows. A semi-empirical correlation was developed for the dual-scale medium which allows prediction of the permeability of hexagonal arrays of fiber tows from a knowledge of their inter- and intra-tow pore volume fractions, the type of intra-tow packing, and the diameter of intra-tow filaments. According to the Papathanasiou analytical solution, the overall permeability of such a dual-scale medium (K_p) is determined by liquid volumes passing through the inter- and intra-tow regions. The latter is related to the permeability of the tow itself (K_{tow}), while the former is related to the permeability of the system with the same inter-tow void volume fraction but made up of impermeable tows (K_s). K_{tow} and K_s are functions of the intra-void volume fraction (ϕ_t) and inter-tow void volume fraction (ϕ_i), respectively. The semi-analytical empirical correlation for K_p is of the form

$$K_p = K_s\left(1 + 2.67\left(\frac{K_{tow}}{K_s}\right)^{0.89}\right), \quad [18]$$

where K_{tow} and K_s are calculated using Gebart's permeability model (1992) as

Table V. Some Micro-geometrical Properties of the Preform and Comparison of the Dual-Scale Permeabilities Obtained Using the Papathanasiou Model and the Single-Scale Permeability Obtained Using the Kozeny-Carman Model

Shape of Tows	Ellipse
Major axis of ellipse	844.64 μm
Minor axis of ellipse	185.65 μm
Fiber diameter	11 μm
ϕ_t	0.24
ϕ_i	0.54
K_s	3.194 E−09 m^2
K_{tow}	2.471 E−15 m^2
K_p	3.194 E−09 m^2
$K_{Kozeny\text{-}Carman}$	1.506 E−12 m^2

$$K = \frac{16}{9\pi\sqrt{2}} \left[\sqrt{\frac{1-\phi_{max}}{1-\phi}} - 1 \right]^{2.5} R^2. \qquad [19]$$

Here, K is the permeability, ϕ is the void volume fraction of the preform, and R is the fiber or tow radius. (Note that the tow radius was half of the tow 'diameter,' which was obtained as the average of the major and minor axes dimensions of the mostly elliptical tows.) ϕ_{max}, the porosity at maximum packing, is different for different types of packing (*i.e.*, the hexagonal or square types).[63]

Empirical measurements on void volume as a fraction of the preform volume (*i.e.*, average void volume fraction) furnish a value of about 0.65. Microscopic analysis of the fabric filaments revealed the average fiber diameter to be 10 to 12 μm. The calculated permeabilities using the Papathanasiou model are presented in Table V. It is noted from Table V that K_{tow} is very small in comparison to K_s and $K_p \cong K_s$. This suggests that very small amount of liquid will pass through the tows during transverse flows. On the other hand, a comparison between the permeability predicted by Kozeny-Carman equation, with the assumption of the preform being a single-scale porous medium, and K_p, derived from the equations for dual-scale preforms proposed by Papathanasiou, shows three orders of magnitude difference between these two models (Table V). This implies that the gaps between tows cause the permeability to shoot up and thus play an important role in facilitating melt flow in the dual-scale preforms.

REFERENCES

1. R.S. Parnas and J.F.R. Phelan: *SAMPE Quarterly*, 1990, vol. 22 (2), pp. 53–60.
2. W.P. Benjamin and S.W. Beckwith, eds.: *Resin Transfer Molding, SAMPE Monograph No. 3*. 1999, SAMPE, USA.
3. S. Suresh, A. Mortensen, and A. Needleman: *Fundamentals of Metal-Matrix Composites*, Butterworth-Heinemann, Stoneham, 1993.
4. H. Tan and K.M. Pillai: *Compos. A*, 2012, vol. 43, pp. 1–13.
5. K.M. Pillai: *J. Compos. Mater.*, 2004, vol. 28 (23), pp. 2097–118.
6. A.W. Chan and R.J. Morgan: *Polym. Compos.*, 1993, vol. 74, pp. 335–40.
7. C. Binetruy, B. Hilaire, and J. Pabiot: *J. Compos. Mater.*, 1998, vol. 32 (3), pp. 223–45.
8. Y.D. Parseval, K.M. Pillai, and S.G. Advani: *Transp. Porous Media*, 1997, vol. 27, p. 243.
9. J. Bréard, Y. Henzel, F. Trochu, and R. Gauvin: *Polym. Compos.*, 2003, vol. 24 (3), pp. 391–408.
10. B.Z. Babu and K.M. Pillai: *J. Compos. Mater.*, 2004, vol. 38 (1), pp. 57–79.
11. H. Tan, T. Roy, and K.M. Pillai: *Compos. A*, 2007, vol. 38 (8), pp. 1872–92.
12. C. Lekakou and M.G. Bader: *Compos. A*, 1998, vol. 29 (1–2), pp. 29–37.
13. R.B. Dessenberger and C.L. Tucker: *Polym. Compos.*, 1995, vol. 16 (6), pp. 495–506.
14. A.W. Chan and R.J. Morgan: *Polym. Compos.*, 1993, vol. 14 (4), pp. 335–40.
15. K.M. Pillai and S.G. Advani: *J. Compos. Mater.*, 1998, vol. 32 (19), pp. 1753–83.
16. K.M. Pillai: *Compos. Mater.*, 2004, vol. 38, pp. 2097–2118.
17. N. Patel, V. Rohatgi, and L.J. Lee: *Polym. Eng. Sci.*, 1995, vol. 35 (10), pp. 837–51.
18. T.S. Lundstorm: *Void Formation and Transport in RTM*, 1993, Swedish Institute Of Composites.
19. R.C. Peterson and R.E. Robertson: in *Proceedings of the 8th Advanced Composites Conference,* 1992, Chicago, IL.
20. Y.T. Chen, H.T. Davis, and C.W. Macosko: *AIChE J.*, 1995, vol. 41 (10), pp. 2261–73.
21. T.S. Lundström and B.R. Gebart: *Polym. Compos.*, 1994, vol. 15 (1), pp. 25–33.
22. YT Chen, C Macosko, and HT Davis: *AIChE J.*, 1995, vol. 41, pp. 2274–81.
23. V. Rohatgi, N. Patel, and L.J. Lee: *Polym. Compos.*, 1996, vol. 17 (2), pp. 161–70.
24. L. Fong and S.G. Advani: in *Proceedings of International Conference on Composite Engineering ICCE*, 1994, p. 301.
25. C.Y. Chang and L.W. Hourng: *J. Reinf. Plast. Compos.*, 1998, vol. 17 (2), pp. 165–82.
26. M. Lin, H.T. Hahn, and H. Huh: *Compos A*, 1998, vol. 29 (5–6), pp. 541–50.
27. R.V. Mohan, N.D. Ngo, and K.K. Tamma: *Polym. Eng. Sci.*, 1999, vol. 39 (1), pp. 26–43.
28. N. Patel and L.J. Lee: *Polym. Compos.*, 1996, vol. 17 (1), pp. 96–103.
29. N. Patel and L.J. Lee: *Polym. Compos.*, 1996, vol. 17 (1), pp. 104–14.
30. K.M. Pillai and S.G. Advani: in *Proceedings of the 1996 ASME International Mechanical Engineering Congress and Exhibition,* 1996.
31. W.K. Chui, J. Glimm, F.M. Tangerman, A.P. Jardine, J.S. Madsen, T.M. Donnellan, and R. Leek: *SIAM Rev.*, 1997, vol. 39 (4), pp. 714–27.
32. A. Mortensen: *Compr. Compos.*, 2000, vol. 3, pp. 521–54.
33. A. Mortensen, L.J. Masur, J.A. Cornie, and M.C. Flemings: *Metall. Trans. A*, 1989, vol. 20 (11), pp. 2535–47.
34. B. Wang and K.M. Pillai: *Metall. Mater. Trans. A*, 2013, vol. 44A, pp. 5834–52.
35. A.M. Samuel, H. Liu, and F.H. Samuel: *J. Mater. Sci.*, 1993, vol. 28 (24), pp. 6785–98.
36. S.N. Aqida, M.I. Ghazali, and J. Hashim: *Jurnal Teknologi*, 2004, vol. 40 (1), pp. 17–32.
37. A. Mortensen, M.N. Gungor, J.A. Cornie, and M.C. Flemings: *JOM*, 1986, vol. 38 (3), pp. 30–35.
38. T.W. Chou, A. Kelly, and A. Okura: *Composites*, 1985, vol. 16 (3), pp. 187–206.
39. M.C. Flemings: *Solidification Processing*, McGraw-Hill, New York, 1974.
40. S. Ray: *J. Mater. Sci.*, 1993, vol. 28 (20), pp. 5397–5413.
41. D. Emadi, J.E. Gruzleski, and J.M. Toguri: *Metall. Trans. B*, 1993, vol. 24B, pp. 1055–63.
42. M Emamy Ghomy and J Campbell: *Cast Metals*, 1995, vol. 8 (2), pp. 115–22.
43. O. Ilegbusi and J. Yang: *Metall. Mater. Trans. A*, 2000, vol. 31A, pp. 2069–74.
44. A.M. Samuel, A. Gotmare, and F.H. Samuel: *Compos. Sci. Technol.*, 1995, vol. 53, pp. 301–15.
45. S. Long, Z. Zhang, and H.M. Flower: *Acta Metall. Mater.*, 1994, vol. 42 (4), pp. 1389–97.
46. A. Mortensen and J.A. Cornie: *Metall. Trans. A*, 1987, vol. 18A, pp. 1160–63.
47. R Asthana: *Solidification Processing of Reinforced Metals*, Transtech Publishers, Switzerland, 1997 46.
48. O. Ilegbusi and J. Yang: *J. Mater. Process. Manuf. Sci.*, 1999, vol. 8 (2), pp. 106–12.
49. R. Calin, M. Pul, and Z.O. Pehlivanli: *J. Mater. Res.*, 2012, vol. 15 (6), pp. 1057–63.
50. T.M. Liu and C.G. Chao: *Mater. Sci. Eng.*, 1993, vol. 169, pp. 79–84.
51. B.S. Kang, C.W. Won, B.S. Chun, and H.Y. Sohn: *J. Mater. Sci*, 1995, vol. 30 (15), pp. 3883–87.
52. T.P.D. Rajan, R.M. Pillai, and B.C. Pai: *J. Mater. Sci.*, 1998, vol. 35, pp. 3491–3503.
53. C. Garcia-Cordovillaa, E. Louis, and J. Narcisoc: *Acta Mater.*, 1999, vol. 47 (18), pp. 4461–79.
54. R.A. Donahue, F. Church, and R.L. Bebee: in *US Patent Documents*, U.S. patent, 1990.
55. M.H. Mohamed, A.E. Bogdanovich, I. Habil, and L.C. Dickinson: *SAMPE J.*, 2001, vol. 37 (3), pp. 8–17.

56. A.J. Wheeler and A.R. Ganji: *Introduction to Engineering Experimentation*, Prentice Hall, 2010.
57. S. Suresh, A. Mortensen, and A. Needleman: *Fundamentals of Metal Matrix Composites*, Butterworth-Heinemann, Boston, 1993.
58. R. Asthana, P.K. Rohatgi, and S.N. Tewari: *Process. Adv. Mater.*, 1992, vol. 2, pp. 1–17.
59. N. Patel and L.J. Lee: *Polym. Compos.*, 1995, vol. 16 (5), pp. 386–99.
60. R.A. Overfelt and D. Wang: *Int. J. Thermophys.*, 2002, vol. 23, pp. 1063–76.
61. J.E. Schoutens: *J. Mater. Sci.*, 1989, vol. 24 (8), pp. 2681–86.
62. J. Campbell: *Complete Casting Handbook—Metal Casting Processes, Metallurgy, Techniques and Design*, Elsevier, Amsterdam, 2011.
63. T.D. Papathanasiou: *Int. J. Multiph. Flow*, 2001, vol. 27 (8), pp. 1451–61.